ON THE ASSESSMENT OF REACTIVITY EFFECTS DUE TO LOCALISED PERTURBATIONS IN BWR LATTICES

R. van Geemert, F. Jatuff, P. Grimm, R. Chawla*
Paul Scherrer Institute,
CH-5232 Villigen PSI, Switzerland

*Co-affiliation :
Swiss Federal Institute of Technology (EPFL),
CH-1015 Lausanne, Switzerland

Keywords: Reactivity effects, perturbation theory, reactor analysis

ABSTRACT

Optimization criteria for the representability of numerical models for the estimation of relative reactivity changes due to localised perturbations in boiling water reactor (BWR) lattices have been theoretically developed and tested. The validity of the derived theoretical expressions has been assessed for the case of a reactivity perturbation corresponding to the removal of an individual fuel pin from a nominal BWR assembly, thus effectively substituting the pin by water. Such reactivity effects are of importance in the context of evaluating advanced fuel element designs, e.g. those employing part-length rods. Two different geometry models have been implemented for the LWR-PROTEUS critical research facility (full core and a smaller, reduced geometry) using the LWR assembly code BOXER (Paratte, 1996), and calculations have been performed for the nominal cases (all pins present in the central test assembly) and the perturbed cases (individual pins removed). The full core results have been compared with the results of the reduced geometry model with two different boundary conditions (reflective and critical albedo). The comparisons have shown that the results of critical albedo calculations feature superior representability. Differences in relative reactivity effects, with respect to results of the full core calculation, are found to be within the range $\pm 1\%$ to $\pm 4\%$.

1. INTRODUCTION

The accurate estimation of integral reactor physics parameters associated with detailed reactivity balance is of utmost importance for achieving high reliability in fuel design and nuclear power plant operation. From the safety assessment viewpoint, this concerns quantities such as core excess reactivity, shutdown rod worths and reactivity coefficients. Modern boiling water reactor (BWR) fuel assembly designs include complex localised features intended for maintaining a well-determined reactivity balance. For instance, part-length fuel pins (i.e., pins of reduced length, which are placed in the lower part of the assembly such

that the pin is replaced by coolant at the top) serve several purposes, for example to increase the shutdown margin. In this context, it is important to show that one is able to accurately calculate the reactivity differences between a certain nominal BWR lattice and one in which one or more pins are replaced by water. In the consideration of such reactivity changes, one is confronted with a number of difficulties, two of which are:

- The fact that the basic approach generally taken by the fuel designer is to calculate the reactivity effects at the level of a single assembly. Normally, calculations are performed using a two-dimensional neutron transport code with a model of the single assembly, with reflective boundary conditions imposed and a buckling correction introduced to produce a fundamental-mode solution that accounts for the leakage spectrum. However, complex core-follow calculations (three-dimensional, diffusion theory) are necessary afterwards to estimate the actual reactivity effect in the reactor.

- The complexity involved in the experimental validation of the reactivity changes calculated at the assembly level. The "real life" conditions dictating the exact physics of the critical experiments in single zone or driven critical systems can be expected to be significantly different from the conditions assumed in the single assembly calculations.

In Section 2 of this paper, a perturbation theory formalism is set up for enabling a theoretical description of the representability of calculated reactivity worths. From this, straightforward approximative expressions, featuring only unperturbed quantities, are derived for relating reactivity effects as computed (for a given perturbation) in two different geometry models. A very useful spin-off of the formalism is the deduction of an easily calculable ratio that will equal 1 in case of exact representability, allowing the modelling conditions to be optimized before actually initiating the pin removal calculations.

In Section 3, the criteria are tested numerically using PSI's LWR lattice code BOXER for the specific case of pin removal reactivity worth experiments in the LWR-PROTEUS research reactor facility (driven system). The BOXER calculations are based on a full-core model and on a reduced-geometry model consisting only of the central test zone (about 1/40 of the total volume). This test zone contains a central test assembly, which is the subzone in which, for validational purposes, fuel pins are removed and thus the actual reactivity changes are imposed. Two different test zone cases have been investigated: one with reflective boundary conditions and critical buckling, and another with a fixed, externally obtained axial buckling imposed and critical albedo boundary conditions. Results obtained from both these test zone models have been compared with the full-core results for a wide range of different pin removals in order to check the developed criteria. Final conclusions are presented in Section 4.

2. THEORETICAL ANALYSIS OF LOCALISED REACTIVITY PERTURBATIONS

The relative reactivity worths of individual fuel pins provide integral parameters of considerable importance for code validational purposes. These results relate to changes in the

neutron balance at the removed-pin location and its nearby surroundings. In order to calculate individual pin removal reactivity effects, first of all a criticality calculation is performed for the unperturbed situation in which an axial and/or radial buckling iteration occurs for establishing numerical criticality (k_{eff}=1). Subsequently, perturbed calculations are performed in which the contents of the pin removal positions of interest are substituted by water.

2.1 Criticality calculations

In general, the neutronics eigenvalue equation can be written as

$$(\mathbf{L} - \lambda\mathbf{F})\,\underline{\psi} = \underline{0} \tag{1}$$

where the eigenvalue λ is the inverse of the effective multiplication factor of the core and $\mathbf{L}$ and $\mathbf{F}$ are the loss and production operators, respectively. We should realize that, for the unperturbed case, λ is in practice forced to 1 since the system is made critical by adjustment of the driver loading. A *critical state* means that, in each spatial point of the reactor, an exact balance exists between neutron production (i.e. emission by fission, inscatter from higher energy groups or incurrent from surroundings) and neutron loss (i.e. absorption, downscatter to lower energy groups or axial leakage). Thus, in case of criticality, the exact balance equation

$$(\mathbf{L} - \mathbf{F})\,\underline{\psi} = 0\,, \tag{2}$$

is satisfied, the vector notation for $\underline{\psi}$ reflecting the multi-energy group structure for the neutron flux. We recall that in the whole reactor, or full core, model, some spatial material densities are tuned by adjusting the driver loading such that criticality is achieved. However, in the reduced geometry models, the outer regions of the reactor are not modelled, so that the fact that the reduced geometry region is part of a critical system has to be simulated numerically. We will adopt the symbols FC, RG and S, indicating the full core (FC), reduced geometry (RG) and the surroundings (S) of the reduced geometry, such that FC=RG+S. Establishing numerical criticality in the RG core can be accomplished by adjusting the axial and/or radial buckling of the system iteratively until criticality is achieved (k_{eff}=1 with sufficient convergence), thus simulating the exact neutron balance in the system. Obviously, once the RG material compositions are fixed, the radial buckling can be adjusted only by manipulation of the boundary conditions, whereas the axial buckling is simply imposed as a scalar. The question addressed in this study is how to make the simulation such that an optimal match is established between RG and FC regarding relative calculated reactivity changes, and how such a match, or departure from such a match, can be quantified.
Later in this paper, we will speak specifically in terms of the LWR-PROTEUS configuration. This is composed of a central fuel assembly (CA, in which the actual material changes are imposed), a ring of additional fuel assemblies surrounding the central test assembly (such that the CA and the ring together form the test zone TZ) and the remaining part of the total system consisting of buffer, driver and reflector regions.

2.2 Reactivity effect ratios in different geometries from a perturbation theory perspective

Utilizing the adjoint flux shape that satisfies the homogeneous adjoint equation

$$(\mathbf{L}^* - \lambda \mathbf{F}^*)\, \underline{\psi}^* = \underline{0}\,, \tag{3}$$

the exact expression (Lewins, 1965) for the eigenvalue change $\delta\lambda$, due to a spatial material composition change that gives rise to the operator changes $\mathbf{L} \rightarrow \mathbf{L} + \delta\mathbf{L}$, $\mathbf{F} \rightarrow \mathbf{F} + \delta\mathbf{F}$ and thus also to a spatial flux change $\underline{\psi}(\underline{\mathrm{r}}) \rightarrow \underline{\psi}(\underline{\mathrm{r}}) + \delta\underline{\psi}(\underline{\mathrm{r}})$, is

$$\delta\lambda = \frac{\int_{\mathrm{MD}} \underline{\psi}^{*\mathrm{T}} \cdot (\delta\mathbf{L} - \lambda\delta\mathbf{F})\, \underline{\psi}' \mathrm{dV}}{\int_{\mathrm{MD}} \underline{\psi}^{*\mathrm{T}} \cdot \mathbf{F}' \underline{\psi}' \mathrm{dV}}\ , \tag{4}$$

with MD standing for Modelling Domain (MD could be the full core FC, or a reduced-geometry region RG that includes the perturbation). The superscript 'T' indicates that we have to take the transposed form of $\underline{\psi}^*$. Eq.(4) is generally valid in the sense that it gives the eigenvalue change as it will occur in the MD model due to the numerical removal of the fuel pin in that model. Since MD is generally not equal to FC, one must of course expect that the eigenvalue change in MD will definitely not be the same as the eigenvalue change in the FC model. This will be because of a difference in model volume and because of a difference in boundary conditions. For example, if the entire set of spatial and energy-spectrum characteristics of a full core model could be reconstructed exactly in a reduced geometry model, thereby preserving correctness in the renormalised distribution of pin removal worths, the absolute values of the recalculated reactivity changes would of course still be different due to the model volume difference. This is inevitable. The removal of one fuel pin in an assembly will have a larger effect in a reflective assembly model than the removal of the same pin in a full core model. The topic of interest here is to guarantee, in the transition from FC to RG, that the correctness of the renormalised distribution of pin removal worths is preserved, i.e. that between each pair of pin removal positions the ratio of the worths remains practically untouched by the transition from FC to RG. If, by adequate setup of the boundary conditions for the RG model, this can be established, we will have realized optimal representability of the RG model with respect to the FC model. This does not mean that an eigenvalue change calculated in the MD-model will be the same as the eigenvalue change in the FC model, but it does mean that the difference between each *ratio* of two pin worths, as calculated in the RG model and the FC model, will be minimal.
Adopting, for the case of the full core model (i.e. MD=FC), a coarse spatial decomposition between the RG zone and its surroundings S (such that FC=RG+S), expression (4) for the eigenvalue change can be written as

$$\delta\lambda = \frac{\int_{\mathrm{RG}} \underline{\psi}^{*\mathrm{T}} \cdot (\delta\mathbf{L} - \lambda\delta\mathbf{F})\, \underline{\psi}' \mathrm{dV} + \int_{\mathrm{S}} \underline{\psi}^{*\mathrm{T}} \cdot (\delta\mathbf{L} - \lambda\delta\mathbf{F})\, \underline{\psi}' \mathrm{dV}}{\int_{\mathrm{FC}} \underline{\psi}^{*\mathrm{T}} \cdot \mathbf{F}' \underline{\psi}' \mathrm{dV}} \tag{5}$$

Since there is no material composition change in the surroundings, we can assume that the operator change $(\delta\mathbf{L} - \lambda\delta\mathbf{F})$ due to the removal of a pin acts significantly only in the rather direct surroundings of the pin vacancy. These direct surroundings are generally confined to the central assembly but, in any case – even for peripheral positions – they are certainly confined to the test zone region. Therefore, the value of the second integral in the numerator can be expected to be negligible. Further, we emphasize that, due to the fact that the neutron mean free path in a BWR is in the order of a few cm, generally the *major* contributions to the total reactivity effect are confined to a local region consisting of the *direct* surroundings of the position of the removed pin, including the vacancy position itself. We now introduce the notation CA for the central assembly, and stress that the CA is the minimal volume RG in the sense that any RG must be equal to the CA or at least contain the CA. Obviously, in case a pin is removed in the central assembly, we will usually have

$$\int_{\mathrm{FC}} \underline{\psi}^{*\mathrm{T}} \cdot (\delta\mathbf{L} - \lambda\delta\mathbf{F})\, \underline{\psi}'\mathrm{dV} \;\cong\; \int_{\mathrm{V_{CA}}} \underline{\psi}^{*\mathrm{T}} \cdot (\delta\mathbf{L} - \lambda\delta\mathbf{F})\, \underline{\psi}'\mathrm{dV} \tag{6}$$

Thus, we obtain

$$\delta\lambda \cong \frac{\int_{\mathrm{V_{CA}}} \underline{\psi}^{*\mathrm{T}} \cdot (\delta\mathbf{L} - \lambda\delta\mathbf{F})\, \underline{\psi}'\mathrm{dV}}{\int_{\mathrm{V_{FC}}} \underline{\psi}^{*\mathrm{T}} \cdot \mathbf{F}'\underline{\psi}'\mathrm{dV}} \tag{7}$$

In the case of the reduced geometry model, it is clear that also the integral in the denominator can be taken only over the RG region (Of course, we have to realize that other adjoint and normal flux distributions will be obtained from the reduced geometry calculation). As we saw previously, the art of optimizing the reduced geometry calculations basically consists of conditioning the boundary conditions in such a way that $\underline{\psi}^*_{\mathrm{RG}}$ and $\underline{\psi}_{\mathrm{RG}}$ match $\underline{\psi}^*_{\mathrm{FC}}$ and $\underline{\psi}_{\mathrm{FC}}$ as well as possible. In this, it is of course assumed that $\underline{\psi}^*_{\mathrm{FC}}$ and $\underline{\psi}_{\mathrm{FC}}$ have been obtained in a calculational model that represents the optimum that can be achieved numerically from a representability point of view (or, in a more basic formulation, that $\underline{\psi}^*_{\mathrm{FC}}$ and $\underline{\psi}_{\mathrm{FC}}$ match $\underline{\psi}^*_{\mathrm{real}}$ and $\underline{\psi}_{\mathrm{real}}$ as closely as possible). For the ratios of calculated reactivity effects as considered for the RG model and the FC model (with $\mathrm{V_{RG}} \geq \mathrm{V_{CA}}$), we can derive:

$$\frac{\Delta\rho_{\mathrm{RG}}}{\Delta\rho_{\mathrm{FC}}} \;\cong\; \frac{\int_{\mathrm{V_{FC}}} \underline{\psi}^{*\mathrm{T}}_{\mathrm{FC}} \cdot \mathbf{F}'\underline{\psi}_{\mathrm{FC}}'\mathrm{dV}}{\int_{\mathrm{V_{RG}}} \underline{\psi}^{*\mathrm{T}}_{\mathrm{RG}} \cdot \mathbf{F}'\underline{\psi}_{\mathrm{RG}}'\mathrm{dV}} \;\frac{\int_{\mathrm{V_{CA}}} \underline{\psi}^{*\mathrm{T}}_{\mathrm{RG}} \cdot (\delta\mathbf{L} - \lambda\delta\mathbf{F})\, \underline{\psi}_{\mathrm{RG}}'\mathrm{dV}}{\int_{\mathrm{V_{CA}}} \underline{\psi}^{*\mathrm{T}}_{\mathrm{FC}} \cdot (\delta\mathbf{L} - \lambda\delta\mathbf{F})\, \underline{\psi}_{\mathrm{FC}}'\mathrm{dV}} \tag{8}$$

The second quotient consists of a division of two integrals calculated over the same volume. In both integrands, the same operator $(\delta\mathbf{L} - \lambda\delta\mathbf{F})$ occurs, so a variation of this quotient will depend basically only on the degree of matching among the spatial shapes of $\underline{\psi}^*$ and $\underline{\psi}'$ between the RG and the FC model. Further, since $(\delta\mathbf{L} - \lambda\delta\mathbf{F})$ will generally be dominated by the part $\lambda\delta\mathbf{F}$, we can justify the approximation:

$$\frac{\int_{\mathrm{V_{CA}}} \underline{\psi}^{*\mathrm{T}}_{\mathrm{RG}} \cdot (\delta\mathbf{L} - \lambda\delta\mathbf{F})\, \underline{\psi}_{\mathrm{RG}}'\mathrm{dV}}{\int_{\mathrm{V_{CA}}} \underline{\psi}^{*\mathrm{T}}_{\mathrm{FC}} \cdot (\delta\mathbf{L} - \lambda\delta\mathbf{F})\, \underline{\psi}_{\mathrm{FC}}'\mathrm{dV}} \cong \frac{\int_{\mathrm{V_{CA}}} \underline{\psi}^{*\mathrm{T}}_{\mathrm{RG}} \cdot \mathbf{F}\underline{\psi}_{\mathrm{RG}}'\mathrm{dV}}{\int_{\mathrm{V_{CA}}} \underline{\psi}^{*\mathrm{T}}_{\mathrm{FC}} \cdot \mathbf{F}\underline{\psi}_{\mathrm{FC}}'\mathrm{dV}} \tag{9}$$

with the unperturbed fission operator in the integrands on the right-hand side present for preserving the effect of the interface function of $\mathbf{F}$ and $\delta\mathbf{F}$ in the inner product taken over the different energy groups. Since neutrons emerging from fission have a high energy, this emphasizes the importance of the high-energy component(s) in $\underline{\psi}^*$. Further, we assume that the values for the quotients will not be affected significantly if the unperturbed flux rather than the perturbed flux is used, and we arrive at the final approximative expression

$$\frac{\Delta\rho_{\mathrm{RG}}}{\Delta\rho_{\mathrm{FC}}} \;\cong\; \frac{\int_{\mathrm{V_{FC}}} \underline{\psi}^*_{\mathrm{FC}}{}^{\mathrm{T}} \cdot \mathbf{F}\underline{\psi}_{\mathrm{FC}}\mathrm{dV}}{\int_{\mathrm{V_{RG}}} \underline{\psi}^*_{\mathrm{RG}}{}^{\mathrm{T}} \cdot \mathbf{F}\underline{\psi}_{\mathrm{RG}}\mathrm{dV}} \;\frac{\int_{\mathrm{V_{CA}}} \underline{\psi}^*_{\mathrm{RG}}{}^{\mathrm{T}} \cdot \mathbf{F}\underline{\psi}_{\mathrm{RG}}\mathrm{dV}}{\int_{\mathrm{V_{CA}}} \underline{\psi}^*_{\mathrm{FC}}{}^{\mathrm{T}} \cdot \mathbf{F}\underline{\psi}_{\mathrm{FC}}\mathrm{dV}} \tag{10}$$

We stress that, with Eq.(10), we have obtained an approximative expression for $\frac{\Delta\rho_{\mathrm{RG}}}{\Delta\rho_{\mathrm{FC}}}$ that is general and independent of the particular perturbation that is applied. For calculating the ratio $\frac{\Delta\rho_{\mathrm{RG}}}{\Delta\rho_{\mathrm{FC}}}$ in this approximation, only *un*perturbed quantities are needed. In this way therefore, it is possible to obtain an *a priori* estimate for $\frac{\Delta\rho_{\mathrm{RG}}}{\Delta\rho_{\mathrm{FC}}}$ before actually doing any pin removal calculations in the models RG and FC! We emphasize that Eq.(10) is inherently insensitive to whether or not the $\underline{\psi}^*_{\mathrm{RG}}$, $\underline{\psi}^*_{\mathrm{FC}}$, $\underline{\psi}_{\mathrm{RG}}$ and $\underline{\psi}_{\mathrm{FC}}$ are normalized similarly, because of the automatic cancelling of any normalization factor since all of the $\underline{\psi}^*_{\mathrm{RG}}$, $\underline{\psi}^*_{\mathrm{FC}}$, $\underline{\psi}_{\mathrm{RG}}$ and $\underline{\psi}_{\mathrm{FC}}$ occur in both the nominator and the denominator. A natural way of imposing exactly the same normalisation condition on both $\underline{\psi}^*$ and $\underline{\psi}$ is to apply the average power density level normalisation over the smaller of the two system volumes, i.e. over $\mathrm{V_{RG}}$, so that:

$$\begin{cases} \underline{\psi}^*_{\mathrm{RG,FC}} := \frac{\underline{\psi}^*_{\mathrm{RG,FC}}}{\int_{\mathrm{V_{RG}}} \underline{1}^{\mathrm{T}}\mathbf{F}\underline{\psi}^*_{\mathrm{RG,FC}}\mathrm{dV}} \\ \underline{\psi}_{\mathrm{RG,FC}} := \frac{\underline{\psi}_{\mathrm{RG,FC}}}{\int_{\mathrm{V_{RG}}} \underline{1}^{\mathrm{T}}\mathbf{F}\underline{\psi}_{\mathrm{RG,FC}}\mathrm{dV}} \end{cases} \tag{11}$$

We can denote the $\underline{\psi}^*_{\mathrm{RG,FC}}$ and the $\underline{\psi}_{\mathrm{RG,FC}}$ that satisfy Eq.(11) as $\underline{\psi}^{(\mathrm{ren.})^*}_{\mathrm{RG,FC}}$ and $\underline{\psi}^{(\mathrm{ren.})}_{\mathrm{RG,FC}}$, respectively. With this renormalisation implemented properly, optimal representability RG$\rightarrow$FC will translate into the second quotient on the right hand side of Eq.(10) being as close to the value 1 as numerically possible. Introducing the notation $\theta_{\mathrm{RG,FC}}$ for this quotient, we emphasize here that the representability optimality condition

$$\theta_{\mathrm{RG,FC}} \;\equiv\; \frac{\int_{\mathrm{V_{CA}}} \left[\underline{\psi}^{(\mathrm{ren.})^*}_{\mathrm{RG}}\right]^{\mathrm{T}} \cdot \mathbf{F}\underline{\psi}_{\mathrm{RG}}{}^{(\mathrm{ren.})}\mathrm{dV}}{\int_{\mathrm{V_{CA}}} \left[\underline{\psi}^{(\mathrm{ren.})^*}_{\mathrm{FC}}\right]^{\mathrm{T}} \cdot \mathbf{F}\underline{\psi}_{\mathrm{FC}}{}^{(\mathrm{ren.})}\mathrm{dV}} \;=\; 1 \tag{12}$$

is a necessary but generally not sufficient condition for optimal representability. In the application of this criterion, it is required that some prior knowledge exists on how to choose or to vary the boundary conditions such that the flux distribution to be obtained in the RG calculation will resemble the one that is obtained in the full core calculation. Once this condition is satisfied, there usually remains a certain degree of freedom, in the sense that the boundary conditions are still slightly variable and thus can be tuned in order to establish a flux match that is optimal within the constraints of the original boundary condition setup.

It should be pointed out here that the strength of this criterion lies in the fact that for the quotient to be 1, not only the flux shapes inside the CA must agree, but implicitly also the flux shape outside the CA because of the imposed flux normalisation that is defined over a reduced geometry region larger than the CA. In the case of LWR-PROTEUS this reduced geometry is a test zone comprising 9 fuel assemblies, the central one of which is the CA. Especially, for the quotient to be 1, the relative importance (dictated by the spatial weighting function $\underline{\psi}^*(\underline{r})\underline{\psi}(\underline{r})$) of the CA with respect to the rest of the RG region must be in close agreement between the RG and FC model. This can only be the case if there is a very good agreement between the overall radial flux curvature in the RG and the FC results. This is important since flux discrepancies in the CA between the RG and FC models are, through the neutronic coupling, significantly influenced by the flux differences in the region surrounding the CA. Due to this, criterion (12) becomes a rather sensitive criterion in the sense that departures from a good overall flux shape agreement in the entire RG region (not only in the CA) are magnified. As will be obvious from the numerical results reported in Section 3, a strong deviation from unity in the value for the representability quotient will overemphasize the departure from optimal transferability. Of course, this sensitivity can only be considered advantageous in the process of representability optimization.

3. TRANSFERABILITY ANALYSIS FOR CALCULATED PIN REMOVAL EFFECTS IN LWR-PROTEUS

In what follows, a representability analysis will be performed for pin removal reactivity worth experiments in the LWR-PROTEUS facility as an example of the applicability of the analytical framework developed in the previous section.

3.1. The LWR-PROTEUS critical facility

The PROTEUS critical facility (Williams, 1998) was reconfigured such as to provide an appropriate LWR spectrum environment to a centrally-located ABB SVEA-96+ fuel element in which measurements are carried out (the “test element”). A SVEA-96+ fuel element consists of 96 fuel pins arranged in four separate sub-bundles, each containing 24 pins on a square pitch around a central water canal. The ^{235}U enrichment varies both axially and radially in the range 2–5 % and some pins contain, additionally, gadolinium as burnable poison in different concentrations (see Fig.1).

The lateral assembly dimensions are about 14 cm across. The test element is surrounded by 8 other identical assemblies, the 3x3 arrangement being located inside an aluminium test tank (Joneja, 2001). Since the elements are 4.5 m in length and the active height of the PROTEUS driver regions is somewhat less than 1 m, the test tank can be driven axially to enable step-wise investigations along the whole length of the test assemblies. This is a special feature of the experiments that is made possible by the unique layout of the facility. In this way, for example, it is possible to study the axial power profile variation across the axial enrichment boundary. The test tank is surrounded by outer radial regions (Joneja, 2001) (the buffer, the D_2O-Driver, the graphite-driver and a graphite reflector) that govern the reactor criticality, thus allowing experiments for a wide range of test lattice k_∞ values. The reactor

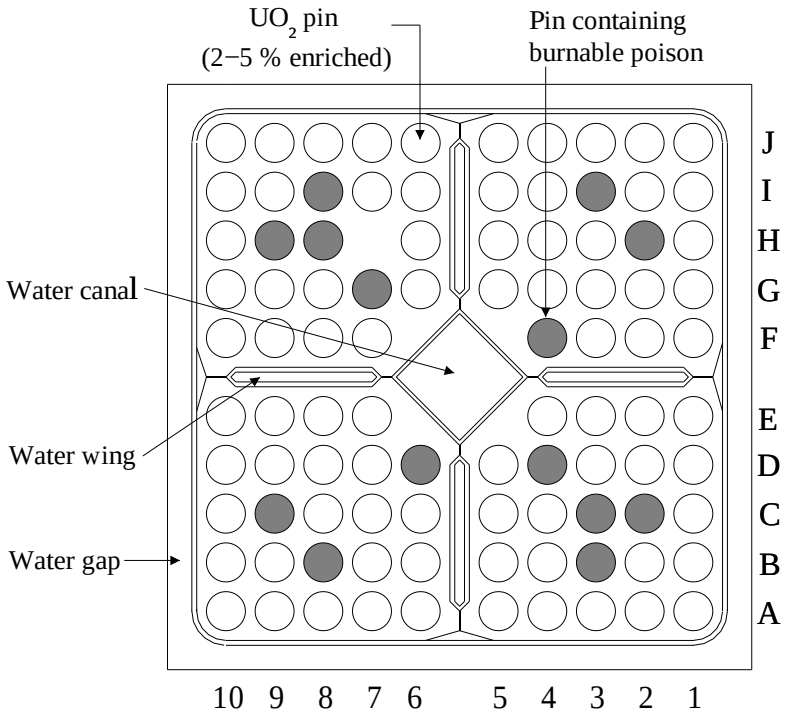

Figure 1 SVEA-96+ assembly geometry (as in LWR-PROTEUS Core 1A), in which the removal of UO_2 pin H7 is illustrated.

instrumentation channels, as well as the control and safety systems, are located in the outer regions, so that the experiments at the centre can be performed under “clean” conditions. The calculated and experimental results that have been used in this study are those for the LWR-PROTEUS Core 1A configuration, in which the conditions in a BWR moderated with cold water are simulated.

3.2 Pin removal worth calculations and their normalisation

Examples of assembly codes that are being validated in the LWR-PROTEUS programme are CASMO-4, HELIOS and BOXER. For the pin removal worth calculations, the axial and radial bucklings are kept fixed at the critical values obtained in the unperturbed calculation. Finally, a reactivity change is calculated as the difference between a reactivity value obtained for a perturbed case and the reactivity value obtained for the unperturbed case (the latter will be zero because of the enforced criticality). The sign of the reactivity is negative in case of the removal of a fuel pin and positive in case of the removal of a burnable absorber pin. The fuel pin reactivity worth distribution can, from a neutronics point of view, be regarded as a kind of importance distribution determined by the material compositions of the fuel pins (i.e. enrichment level, amount of absorbing material in case of Gd-pins, etc.) and the spatial shape of the neutron flux distribution. Since, in general, axial homogeneity can be assumed and the fuel pins’ importances are determined partially by their position in

a radially organized lattice, a high degree of quality in the reconstruction of the *radial* flux and power distribution is a prerequisite for a well-qualified numerical representation of the fuel pin reactivity worth map.

In the LWR-PROTEUS calculational scheme, a distinction is made between full core, test zone and single assembly calculations of which the latter two are reduced geometry calculations (see Fig.2). Of course, models defined in different volumes will yield different values for a calculated reactivity effect, such that eventually in the validation process one should compare only the *ratios* between different pin removal effects calculated within the same model. A possible way to do this is to *renormalize* each set of pin removal worths such that the sum of their absolute values equals unity. These renormalised pin removal worth distributions can then be used for the investigation of intercalculational representability properties.

With regard to a high-quality reconstruction of the radial flux distribution in the test zone, particularly in the central assembly region, realistic results can of course be expected from the FC calculations, whereas it is not *a priori* clear whether this will be the case for the test zone (TZ) and the central assembly (CA) calculations. As already indicated at the end of Section 2.2, obtaining a realistic renormalised calculated pin removal worth requires an appropriate choice to be made for the type of boundary conditions implemented at the edges. In LWR-PROTEUS Core 1A, especially the peripheral and corner components of the radial fuel pin reactivity worth distribution in the central assembly are rather sensitive to the type of boundary conditions implemented at the cartesian edges of the modelled system (reflected assembly or test zone). The reason for this is that boundary conditions significantly affect the global radial neutron flux curvature which, in turn, partially determines the reactivity importance of the different radially distributed fuel pins. For the reduced geometry models, artificial manipulation of the boundary conditions is the only way to simulate the global radial flux curvature correctly. The real radial flux shape can be thought of as a superposition of this global radial flux shape and the local radial flux variations that are due to the gradients in material densities across the different pins within the assembly lattice.

3.3 Boundary conditions in reduced geometry calculations

For reduced geometry calculations to produce reality-representative results, the global flux shape in the CA region calculated with this geometry needs to match the *real* shape. Of course, the question whether this is generally the case cannot be answered in a perfect way since the *real* global flux shape can never be measured. However, the next best answer emerges from a comparison of the flux shape contained, say, in a TZ calculation with that obtained from an FC calculation.

3.3.1 Reflective boundary conditions

In the reality of the Core 1A test zone, there is an overall decrease in the flux and power distributions, even though all the 9 elements in the test zone are basically identical. The basic flaw associated with the application of *reflective* boundary conditions consists of the

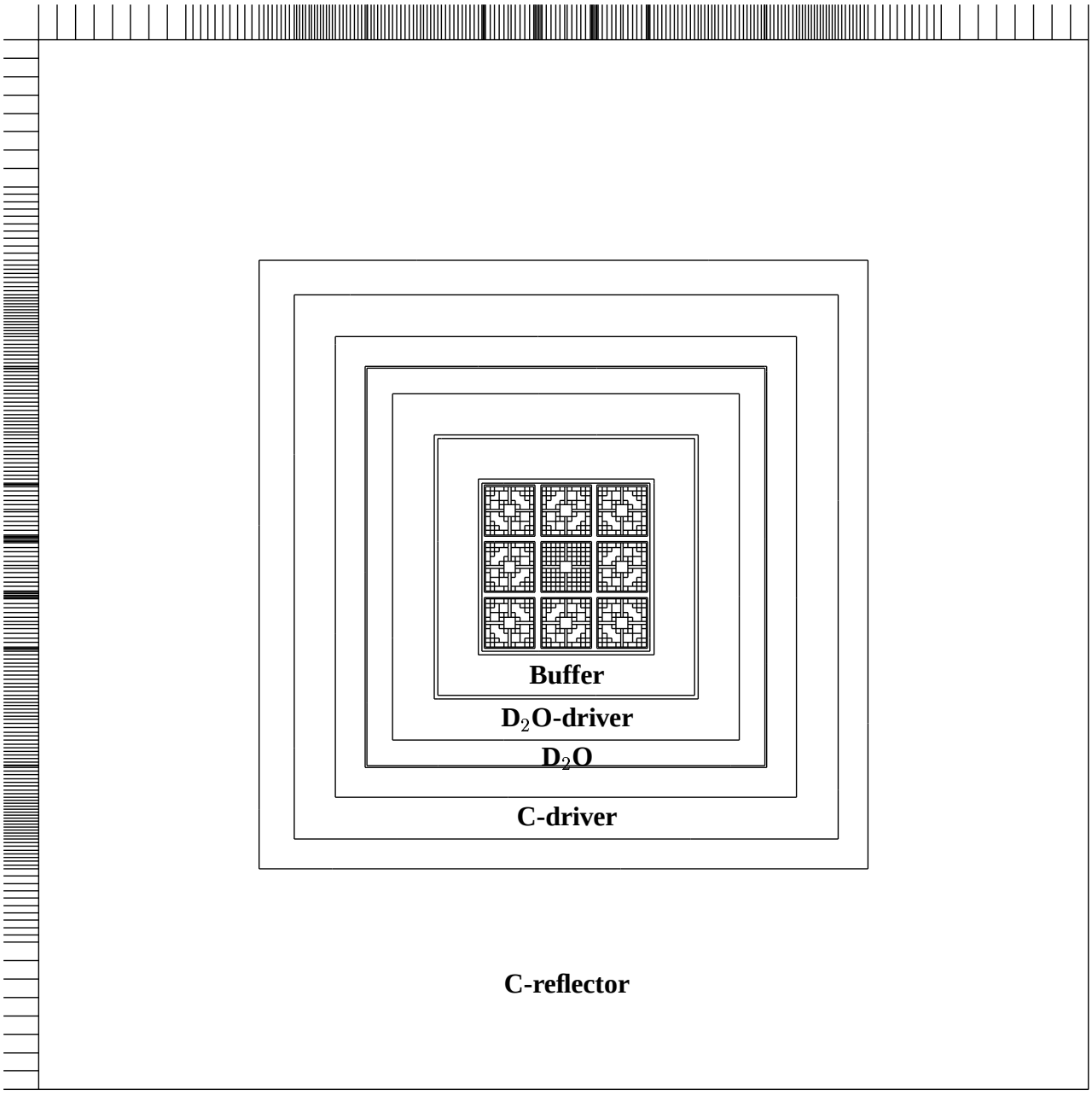

Figure 2 The BOXER cartesian model of the full PROTEUS core (FC). Clearly visible is the part corresponding to the reduced geometry model of the test zone (TZ), consisting of the central assembly (CA) (which represents a reduced geometry model in itself) surrounded by its eight neighbours.

inability to account numerically for the overall variations in the global flux and power distributions. Fundamentally and in real life, a criticality search consists of the adjustment of the amount and position of materials in the system such that an exact neutron balance is established and the system is made critical. This adjustment effectively determines the extent to which the flux distribution is *curved* radially and axially. In the two-dimensional FC calculations, the compositions, volumes and location of the different material zones in PROTEUS are assumed to be modelled adequately and in correspondence with the real-life critical configuration (with the number of fuel rods in the driver region required for criticality quantified correctly). Assuming that the axial and radial flux curvatures can be decoupled, the calculated radial flux curvature should then be optimally representative of the real radial flux curvature. This is necessary since the latter partially determines the relative importance of central and peripheral fuel pins.

Clearly, when implementing *reflective* boundary conditions in the reduced geometry model and thus *artificially eliminating* the occurrence of the peripheral decrease towards the edges of the reduced geometry, exact results can be expected only in the hypothetical case of an *infinite* lattice of fuel elements. In practice, the use of reflective boundary conditions needs to be restricted to the modelling of components that have volumes small enough to prevent any significant radial flux curvature from being noticeable. From the FC global flux shape across the central test zone, it is obvious that such a condition is met neither in the case of the test zone nor in that of the central assembly region.

3.3.2 Iterating on the albedo

In the analysis of LWR-PROTEUS Core 1A, it is seen that, with reflective boundary conditions, the removal worths of peripheral pins will be relatively overpredicted with respect to those of the more centrally located pins because of the systematic negligence of the global decrease of the neutron flux towards the edges. In order to obtain more representative (radial) pin removal reactivity effect maps for the CA in reduced geometry calculations, the partial fuel pin worth variations due to the radial flux curvature can be incorporated by using an externally calculated fixed axial buckling corresponding to the neutronic height of the system and criticality-iterating on the boundary conditions (and thus on the radial flux curvature). Since changes in the neutron spectrum between the CA and the outer eight assemblies are minimal, the three-dimensional neutron flux $\underline{\psi}$ in the CA should be expected to feature axial and radial curvatures that are very nearly equal to those for the central assembly in the FC model. This can be done by varying the *albedo* at the RG boundaries. Implicitly, this means iterating on the radial flux curvature rather than on the axial flux curvature. This approach can be expected to produce more realistic results because, since the fuel pins are positioned in a two-dimensional lattice parallel to the computationally modelled one, radial flux curvature will have a far more significant influence on the renormalised spatial pin worth distribution than axial flux curvature, the effect of which is assumed to be homogeneous among the fuel pins and to more or less average out in the final renormalization. In BOXER, the option is offered to conduct criticality calculations by iterating on the albedo factor to be applied at the boundaries (thus indeed basically iterating on the radial flux curvature) rather than to implement fixed reflective boundary conditions and performing a buckling search. In this BOXER option, a single albedo value is applied to all the groups, so that the energy spectrum is frozen and effectively only the spatial (radial) shapes

of the group-dependent fluxes are modified.

A comparison between the three different models FC (Full Core), RTZ (Reflected Test Zone) and CATZ (Critical Albedo Test Zone) is given in Fig.3, in which $\psi^*_{\mathrm{RTZ}}\psi_{\mathrm{RTZ}}$, $\psi^*_{\mathrm{FC}}\psi_{\mathrm{FC}}$ and $\psi^*_{\mathrm{CATZ}}\psi_{\mathrm{CATZ}}$ represent the global importance functions generated by reflected test zone, full core and critical albedo calculations, respectively. Because of the unillustrated presence of a buffer region that directly surrounds the test zone, the FC global importance shape $\psi^*_{\mathrm{FC}}\psi_{\mathrm{FC}}$ differs slightly from the cosinusoidal curve featured by $\psi^*_{\mathrm{CATZ}}\psi_{\mathrm{CATZ}}$ near the edge of the test zone. Since the total integrated importance is required to be the same for all models, an absence of global radial flux curvature, as featured in the RTZ solution, lowers the relative importance of the CA region in the test zone.

3.4 Application of the optimal-representability criterion

In this section we provide numerical examples for the validity of the analytical framework by reporting results for LWR-PROTEUS Core 1A as obtained with BOXER. We note that the BOXER calculations featured the use of 24 energy groups. However, a convenient part of the output generally features a listing of region-averaged *two*-group quantities like the region-averaged two-group fission and absorption cross sections and the region-averaged two-group neutron flux, along with a listing of the volumes of the different regions. Realizing that, in the particular two-group picture adopted here, all neutrons emerging from fission belong to group 1 (the fast group), $\mathbf{F}$ can be written in a two group-wise sense as

$$\mathbf{F} = \begin{pmatrix} \nu\Sigma_{\mathrm{F1}} & \nu\Sigma_{\mathrm{F2}} \\ 0 & 0 \end{pmatrix} \tag{13}$$

due to which we obtain

$$\frac{\Delta\rho_{\mathrm{TZ}}}{\Delta\rho_{\mathrm{FC}}} \cong \frac{\int_{\mathrm{V_{FC}}} \psi^*_{\mathrm{1FC}} \left(\nu\Sigma_{\mathrm{F1}}\psi_{\mathrm{1FC}} + \nu\Sigma_{\mathrm{F2}}\psi_{\mathrm{2FC}}\right) \mathrm{dV}}{\int_{\mathrm{V_{TZ}}} \psi^*_{\mathrm{1TZ}} \left(\nu\Sigma_{\mathrm{F1}}\psi_{\mathrm{1TZ}} + \nu\Sigma_{\mathrm{F2}}\psi_{\mathrm{2TZ}}\right) \mathrm{dV}} \; \frac{\int_{\mathrm{V_{CA}}} \psi^*_{\mathrm{1TZ}} \left(\nu\Sigma_{\mathrm{F1}}\psi_{\mathrm{1TZ}} + \nu\Sigma_{\mathrm{F2}}\psi_{\mathrm{2TZ}}\right) \mathrm{dV}}{\int_{\mathrm{V_{CA}}} \psi^*_{\mathrm{1FC}} \left(\nu\Sigma_{\mathrm{F1}}\psi_{\mathrm{1FC}} + \nu\Sigma_{\mathrm{F2}}\psi_{\mathrm{2FC}}\right) \mathrm{dV}} \tag{14}$$

For the numerical evaluation of the integrals occurring in Eq. (14) based on the normal BOXER output, we note that the two-group region averages can be applied in an approximation in which for each region i the subintegral $\int_{\mathrm{V_i}} \psi^*_1 \left(\nu\Sigma_{\mathrm{F1}}\psi_1 + \nu\Sigma_{\mathrm{F2}}\psi_2\right) \mathrm{dV}$ can be approximated as

$$\int_{\mathrm{V_i}} \psi^*_1 \left(\nu\Sigma_{\mathrm{F1}}\psi_1 + \nu\Sigma_{\mathrm{F2}}\psi_2\right) \mathrm{dV} \cong \mathrm{V_i} \langle\psi^*_1\rangle_{\mathrm{i}} \langle\nu\Sigma_{\mathrm{F1}}\psi_1 + \nu\Sigma_{\mathrm{F2}}\psi_2\rangle_{\mathrm{i}} \tag{15}$$

Further, assuming a sufficient degree of self-adjointness for the transport operator for the fast group, we can assume that $\underline{\psi}^*(\underline{\mathrm{r}})$ has roughly the same shape as $\underline{\psi}(\underline{\mathrm{r}})$. In this 2-group approximation we then obtain the following expression for $\frac{\Delta\rho_{\mathrm{TZ}}}{\Delta\rho_{\mathrm{FC}}}$:

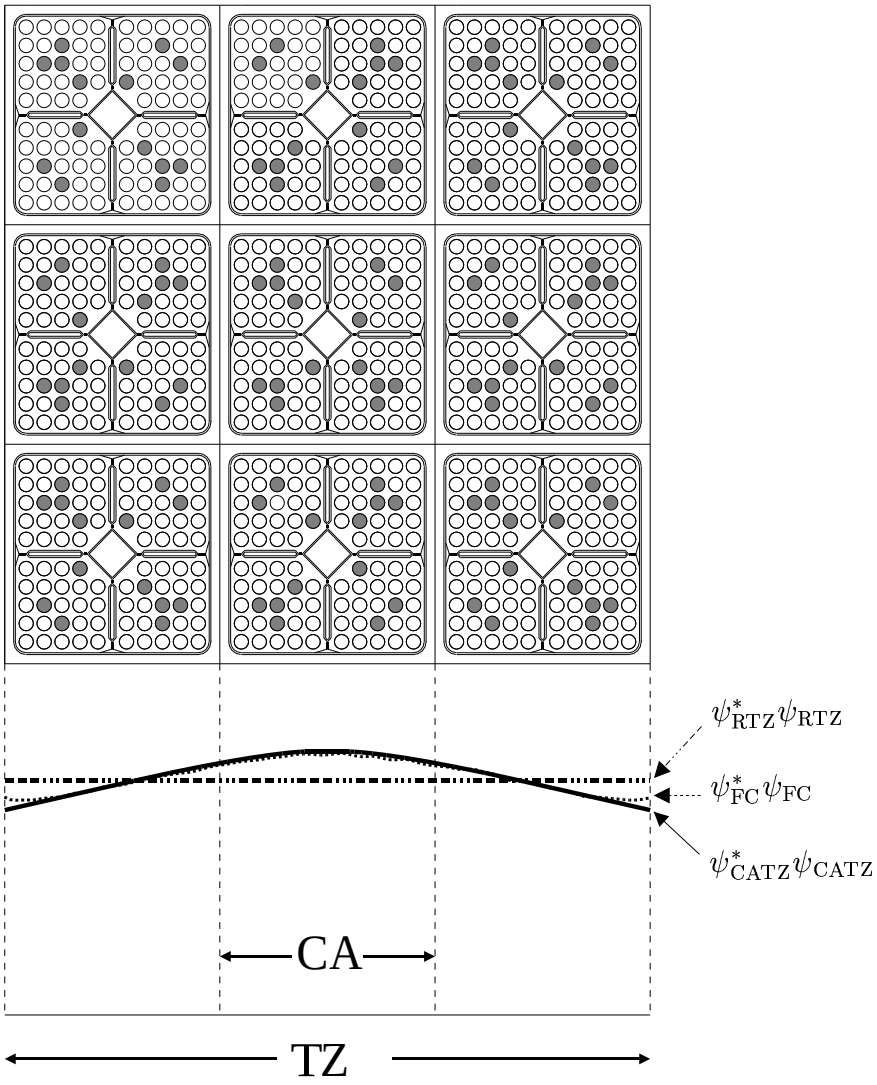

Figure 3 Illustration of global importance variation within a test zone region characteristic of LWR-PROTEUS Core 1A, as a function of the choice for the boundary conditions. $\psi^*_{\mathrm{RTZ}}\psi_{\mathrm{RTZ}}$, $\psi^*_{\mathrm{FC}}\psi_{\mathrm{FC}}$ and $\psi^*_{\mathrm{CATZ}}\psi_{\mathrm{CATZ}}$ represent the global importance functions generated by reflected test zone, full core and critical albedo models, respectively. Since the total integrated importance is required to be the same for all models, an absence of global radial flux curvature, as featured in the RTZ solution, lowers the relative importance of the CA region in the test zone.

$$\frac{\Delta\rho_{\rm TZ}}{\Delta\rho_{\rm FC}} \cong \frac{\sum_{\rm i\in FC} {\rm V_i}\langle\psi_{\rm 1FC}\rangle_{\rm i}\langle\nu\Sigma_{\rm F1}\psi_{\rm 1FC}+\nu\Sigma_{\rm F2}\psi_{\rm 2FC}\rangle_{\rm i}}{\sum_{\rm i\in TZ} {\rm V_i}\langle\psi_{\rm 1TZ}\rangle_{\rm i}\langle\nu\Sigma_{\rm F1}\psi_{\rm 1TZ}+\nu\Sigma_{\rm F2}\psi_{\rm 2TZ}\rangle_{\rm i}} \frac{\langle\psi_{\rm 1TZ}\rangle_{\rm CA}\langle\nu\Sigma_{\rm F1}\psi_{\rm 1TZ}+\nu\Sigma_{\rm F2}\psi_{\rm 2TZ}\rangle_{\rm CA}}{\langle\psi_{\rm 1FC}\rangle_{\rm CA}\langle\nu\Sigma_{\rm F1}\psi_{\rm 1FC}+\nu\Sigma_{\rm F2}\psi_{\rm 2FC}\rangle_{\rm CA}} \tag{16}$$

In the case of the BOXER-based analysis of LWR-PROTEUS Core 1A, the *predicted* $\frac{\Delta\rho_{\rm TZ}}{\Delta\rho_{\rm FC}}$ ratio obtained by application of Eq.(16) turned out to give a good agreement with the *observed* average ratio between $\Delta\rho_{\rm TZ}$ and $\Delta\rho_{\rm FC}$. The comparison for Core 1A between average predicted and explicitly calculated $\frac{\Delta\rho_{\rm TZ}}{\Delta\rho_{\rm FC}}$'s is given in Table I.

Table I Comparison between predicted and the average of the directly calculated ratios $\frac{\Delta\rho_{\rm TZ}}{\Delta\rho_{\rm FC}}$ for BOXER-modelled pin removal reactivity effects in LWR-PROTEUS Core 1A.

Case	$\left(\frac{\Delta\rho_{\rm TZ}}{\Delta\rho_{\rm FC}}\right)_{\rm RTZ}$	$\left(\frac{\Delta\rho_{\rm TZ}}{\Delta\rho_{\rm FC}}\right)_{\rm CATZ}$
Predicted	1.29	1.91
Calculated	1.27	1.93

The TZ results considered above were obtained under different conditions, fixed reflective boundary conditions and critical albedo at the boundary. These results confirm the comment added to the Fig. 3 caption, stating that since the total integrated importance is required to be the same for both models, the absence of global radial flux curvature lowers the relative importance of the CA region in the test zone. It is because of this effect that the absolute values of the calculated reactivity effects are lower for the RTZ model than for the CATZ case. In Figs. 4 and 5, the numerically obtained values for $\left(\frac{\Delta\rho_{\rm TZ}}{\Delta\rho_{\rm FC}}\right)_{\rm RTZ}$ and $\left(\frac{\Delta\rho_{\rm TZ}}{\Delta\rho_{\rm FC}}\right)_{\rm CATZ}$ are given in the form of CA maps for the different pin removal cases. It has turned out that for reduced geometry models, fixing the axial buckling and performing an albedo iteration (equivalent to a radial buckling iteration) yields better representability with respect to the full core results. That this is indeed the case is illustrated in Figs. 6 and 7, in which the representabilities of the two BOXER-based TZ models are compared in terms of individual renormalised $\frac{\Delta\rho_{\rm TZ}}{\Delta\rho_{\rm FC}}$ ratios. All four corner pins of the central assembly have been included in the set of pin removals considered, the calculated reactivity effects being derived from unperturbed and perturbed $k_{\rm eff}$ values.
In Table II, the standard deviations $\sigma\left(\frac{\Delta\rho_{\rm TZ}}{\Delta\rho_{\rm FC}}\right)$ are listed for the two different cases. Added are the corresponding values for the general representability ratio $\theta_{\rm RG,FC}$ for the two listed cases.

Table II The standard deviations $\sigma\left(\frac{\Delta\rho_{\rm TZ}}{\Delta\rho_{\rm FC}}\right)$ and representability ratios θ for the two different cases.

case	RTZ	CATZ
$\sigma\left(\frac{\Delta\rho_{\rm TZ}}{\Delta\rho_{\rm FC}}\right)$	0.0597	0.0064
$\theta_{\rm case,FC}$	0.6244	0.9997

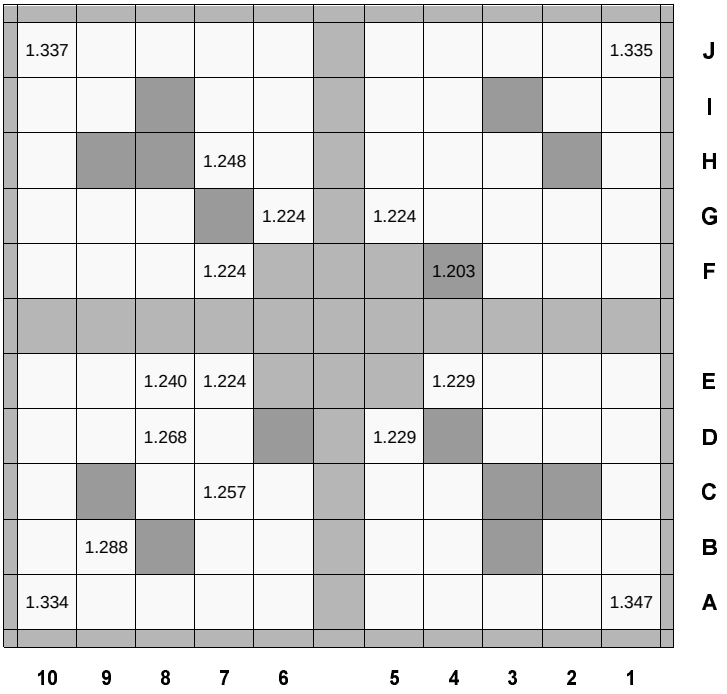

Figure 4 CA map containing the BOXER RTZ-results in terms of individually obtained ratios $\left(\frac{\Delta\rho_{\mathrm{TZ}}}{\Delta\rho_{\mathrm{FC}}}\right)_{\mathrm{RTZ}}$.

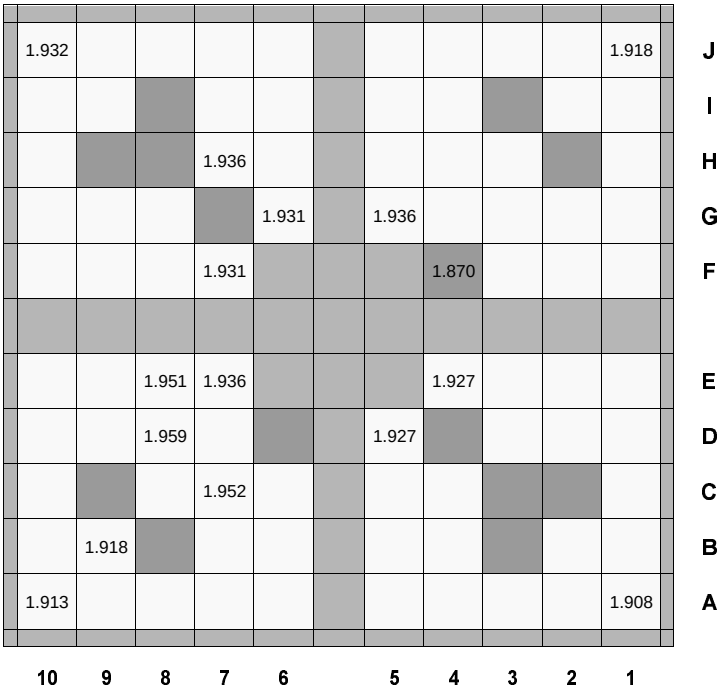

Figure 5 CA map containing the BOXER CATZ model results in terms of individually obtained ratios $\left(\frac{\Delta\rho_{\mathrm{TZ}}}{\Delta\rho_{\mathrm{FC}}}\right)_{\mathrm{CATZ}}$.

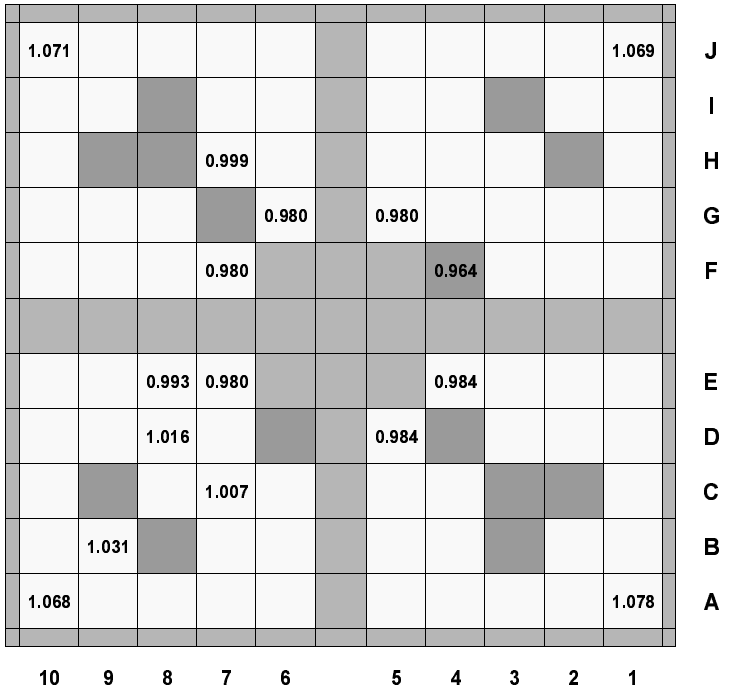

Figure 6 Representability map for the BOXER RTZ model in terms of individual *renormalised* $\frac{\Delta\rho_{\mathrm{TZ}}}{\Delta\rho_{\mathrm{FC}}}$ ratios.

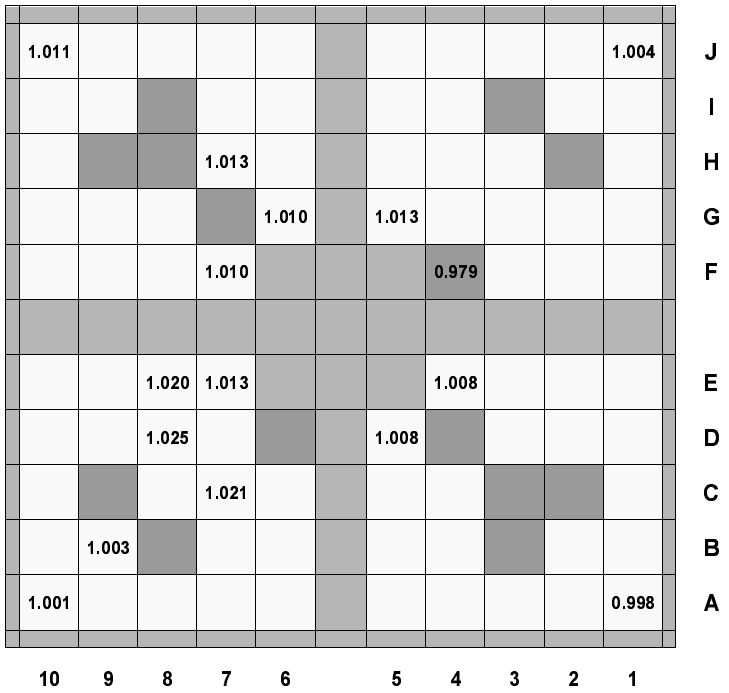

Figure 7 Representability map for the BOXER CATZ model in terms of individual *renormalised* $\frac{\Delta\rho_{\mathrm{TZ}}}{\Delta\rho_{\mathrm{FC}}}$ ratios.

It is seen that, in the case of the variable albedo model, the standard deviation is less than 0.7 %, i.e. an order of magnitude smaller than in the RTZ case. Clearly, the θ-value is much closer to unity in the CATZ (critical albedo) case, indicating its superior representability.

4. CONCLUSIONS

A theoretical study has been presented for evaluating the representability of alternative geometry models for the calculation of localised reactivity perturbation effects in BWR lattices. The theoretical framework has been tested for the particular case of pin removal worths in the context of an experimental project being carried out at a driven critical facility, viz. LWR-PROTEUS. Measurements are performed with very high precision in the experimental programme, and it is extremely important to establish optimal representability of the calculated results with respect to the real-life multizone nature of the reactor configuration in order to identify trends of a few percent.

In this study, emphasis has been laid on the investigation of the influence of different types of boundary conditions implemented at the system edges in reduced geometry calculations. A perturbation theory formalism has served as basis for describing the physics of pin removals and the quantification of representability. It has thus been possible to derive approximative expressions for the *a priori* prediction of the ratios between calculated unnormalized pin removal reactivity effects in different geometries and with different boundary condition types. The validity of these expressions has been supported by comparison with detailed calculational results, which yielded very good agreement. An important spin-off of the perturbation theory formalism has been the derivation of an easily calculable ratio that must be close to unity in case of optimal representability. The computation of this ratio only requires the results of two unperturbed calculations, viz. for the two models of interest.

A significant finding from this analytical/numerical study is that the presence of peripheral pins in a given validational set of pin removals demands an explicit consideration of the *global radial flux curvature* across the central test assembly. In the case of LWR-PROTEUS Core 1A, an experimental configuration with a significant positive curvature across the central test assembly, not doing so (for instance in the case of applying reflective boundary conditions) has been shown to result in corner pin reactivity effects being considerably overpredicted, accompanied of course by a relative underprediction of removal worths for centrally located pins.

ACKNOWLEDGEMENTS

The LWR-PROTEUS programme is being conducted jointly by PSI and the Swiss Nuclear Utilities (UAK), with specific contributions from Elektrizitätsgesellschaft Laufenburg (EGL) and Aare-Tessin AG für Elektrizität (ATEL). We are particularly grateful to H. Achermann and T. Williams (EGL), H. Fuchs (ATEL), G. Meier (KKG), R. Stratton (NOK), D. Furtado (KKM), W. Kröger and R. Brogli (PSI) for their strong support of the experiments.

REFERENCES

O. Joneja, M. Plaschy, F. Jatuff, A. Lüthi, M. Murphy, R. Seiler, R. Chawla, 2001. “Validation of an MCNP4B Whole-Reactor Model for LWR-PROTEUS using ENDF/B-V, ENDF/B-VI and JEF-2.2 Cross-Section Libraries”, Annals of Nuclear Energy, Vol. 28, No. 7, pp. 701-713.

J. Lewins, 1965, “Importance: the Adjoint Function”, Pergamon Press Ltd.

J.M. Paratte *et al.*, 1996, “ELCOS, The PSI Code System for LWR Core Analysis. Part II: User’s Manual for the Fuel Assembly Code BOXER”, PSI Bericht Nr. 96-08.

T. Williams, R. Chawla, P. Grimm, O. Joneja, R. Seiler, A. Ziver, 1998. “New Experiments at a Zero-Power Facility Using Power Reactor Fuel”, Proceedings of the International Conference on the Physics of Nuclear Science and Technology, pp. 720-727, Long Island (USA).